Frequency support characteristics of grid-interactive power converters based on the synchronous power controller

Weiyi Zhang[1] ✉, *Daniel Remon*[1], *Pedro Rodriguez*[1,2]

[1]*Department of Electrical Engineering, Technical University of Catalonia, Rambla Sant Nebridi, Terrassa, Barcelona 08222, Spain*

[2]*Abengoa Research, Abengoa, Palmas Altas, Sevilla 41014, Spain*

✉ *E-mail: weiyi.zhang@estudiant.upc.edu*

Abstract: Grid-interactive converters with primary frequency control and inertia emulation have emerged and are promising for future renewable generation plants because of the contribution in power system stabilisation. This study gives a synchronous active power control solution for grid-interactive converters, as a way to emulate synchronous generators for inerita characteristics and load sharing. As design considerations, the virtual angle stability and transient response are both analysed, and the detailed implementation structure is also given without entailing any difficulty in practice. The analytical and experimental validation of frequency support characteristics differentiates the work from other publications on generator emulation control. The 10 kW simulation and experimental frequency sweep tests on a regenerative source test bed present good performance of the proposed control in showing inertia and droop characteristics, as well as the controllable transient response.

1 Introduction

The stability of a given electrical power system is dependent on balancing the generation, demand and losses. The estimation of generation and demand plays a decisive role when planning operation schedules for power plants and transmission systems. With continuous penetration of renewables and the expansion of distributed generation plants, central coordination becomes more challenging. Instead, generation and demand with automatic response to voltage and frequency changes becomes a promising solution in the long run with respect to both stability and economy.

In practice, only large power stations comprised of clusters of synchronous generators incorporate a droop mechanism for regulating their generated power as a function of the grid frequency variation. In order to provide frequency and voltage regulation from each interfaced terminal in the modern electrical network, renewable generation plants based on grid-connected converters are also required to interact with the grid and provide frequency and voltage support [1]. As the share of the renewable power generation increases, the impact of the renewables will be more tangible and the role of these plants should be changed [2]. Therefore, the steady-state performance of a grid-connected converter needs to be specified by droop characteristics instead of the maximum power point tracking. Droop control has been well used in microgrids for frequency support in both grid-connected and island mode [3–5]. Further, once the energy reserve is available, the droop algorithm can also be used in large-scale renewable power generation.

In addition to droop control, synthetic inertia techniques have also emerged in order to improve the transient performance of a grid-connected converter, which act as a competitive alternative to the traditional definition of converter dynamics that are characterised by phase-locked loop (PLL) [6] and instantaneous power theory [7]. The dynamics comparison between the inertia emulation control and droop control has been studied in works such as [8, 9].

The idea of specifying the grid-connected converters with inertia and droop characteristics is well accepted because of the successful operation of the traditional power system, which relies on the electromechanical characteristics of the numerous synchronous generators. In detail, the output impedance of a synchronous machine determines its electrical characteristics that contribute to load sharing and voltage droop, and the rotor inertia determines its mechanical characteristics that guarantee the healthy dynamics of the power system. Therefore, the generator emulation control (mainly the emulation of the electromechanical characteristics) has been studied intensively in the past years ever since its first publication [10, 11]. The studies have been conducted from different perspectives such as inertia emulation [12, 13], PLL-less control [14, 15], providing virtual impedance [16–18], adaptive inertial response [19, 20], primary frequency and voltage control [21], stability analysis [22], and design of energy storage [23]. The application scenarios also vary such as the distributed generation [24–30], electric vehicles [21] and high-voltage dc systems [31–34].

The abovementioned works give insightful analysis or constructive implementation proposals on different aspects of generator emulation control, whereas the transient analysis and experimental validation in presence of grid frequency variations are not thoroughly shown. Even if the results shown in [19, 21, 35] have exhibited the frequency support effect under load changes, a quantitative transient relation between the grid frequency and active power is not given and validated.

This paper designs a synchronous power control strategy for grid-connected converters to provide inertia emulation and primary frequency control. An active power loop controller integrating inertia emulation, damping and *P-f* droop control is proposed as a simple design alternative to the typical emulation of the synchronous machine swing equation. Particularly, compared with existing studies, the transient response of the converters in presence of grid frequency changes is studied analytically and validated in experiments in this paper. The controlled grid-connected converter can give frequency support accurately following the specified dynamics, which is in turn determined by the inertia and damping parameters.

The rest of the paper is organised as follows. In Section 2, the general control framework is introduced and the mechanisms of the synchronous power controller are briefly explained. The detailed design of the synchronous active power control loop is presented in Section 3, taking into account the stability and transient response. Simulation and experimental validation are given in Sections 4 and 5 which particularly show the frequency support characteristics of the designed controller, and Section 6 draws the conclusion of the paper.

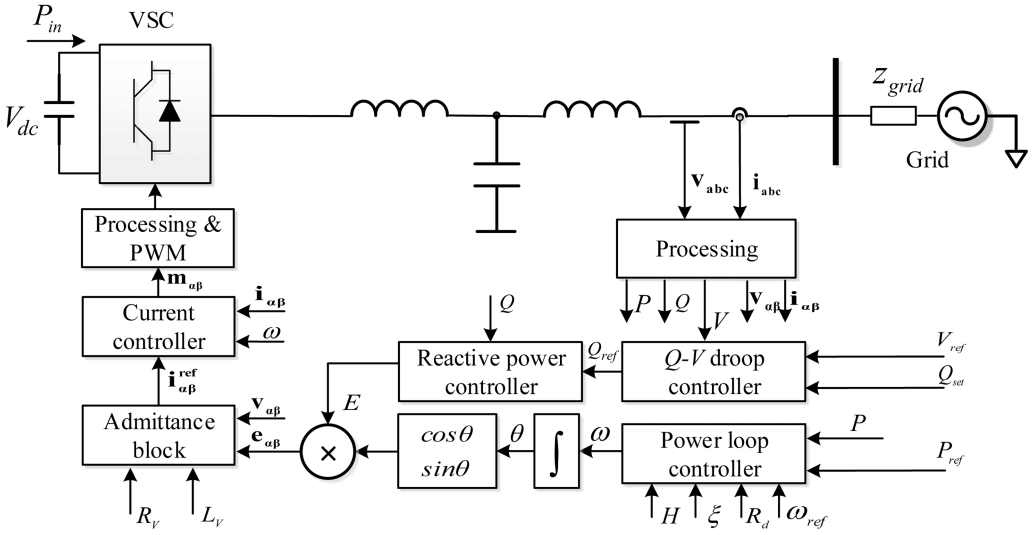

Fig. 1 *Grid-interactive power converters based on the synchronous power controller*

2 SPC-based grid-interactive converters

The grid-interactive converter is controlled based on the general control framework referenced as the synchronous power controller (SPC) [36, 37], which is shown in Fig. 1.

SPC evolves out of the emulation and enhancement of the electromechanical characteristics of synchronous machines. The output impedance and inertia of synchronous machines are both taken into account in the control structure. The virtual admittance combined with the power loop controller can achieve the specified electromechanical characteristics with properly assigned control parameters.

The exchange of active and reactive power between two voltage sources *e* and *v* are written as,

$$P = \frac{EV}{Z}\cos(\phi - \delta) - \frac{V^2}{Z}\cos\phi \tag{1}$$

$$Q = \frac{EV}{Z}\sin(\phi - \delta) - \frac{V^2}{Z}\sin\phi \tag{2}$$

where E and V are the rms of e and v, $Z\angle\phi$ the impedance and δ the phase angle difference between e and v.

For common synchronous machines, considering a mainly inductive output impedance and a small value of δ, (1) and (2) become,

$$P = P_{\max}\delta = \frac{EV}{X}\delta \tag{3}$$

$$Q = \frac{V(E - V)}{X} \tag{4}$$

Synchronous machines regulate the active and reactive power through the governor and exciter, adjusting the speed and voltage, respectively. Similarly, SPC controls the active and reactive power by adjusting θ and E, respectively, such as a synchronous machine, rather than the conventional control of active and reactive power through the decoupling control in rotating frame.

Different from many other methods of generator emulation control, SPC also considers the emulation of the stator. In many low-voltage grids where several converters are connected in parallel, the grid impedance is not necessarily inductive and hard to be estimated. SPC uses a virtual admittance structure to define the output impedance to ensure a high *X*-*R* ratio. Several other advantages of virtual admittance include the current limitation, smooth start-up, easy islanding and parallel operation. In single phase the virtual admittance has the form of,

$$i_{\text{ref}} = \frac{e - v}{R + sL} \tag{5}$$

Equation (5) is a low-pass structure by itself, and does not entail the derivative term for processing the current measurement that is often seen in the virtual impedance structure written as,

$$v_{\text{ref}} = e - i(R + sL) \tag{6}$$

Another advantage of (5) compared with (6) is the simplicity in inner loop tuning, where only a current controller is enough and voltage source fighting is avoided. The current controller can be placed in the stationary frame written as,

$$m_{\alpha\beta} = \frac{1}{v_{\text{dc}}}\left(K_p + K_r\frac{\omega s}{s^2 + \omega^2}\right)(\boldsymbol{i}_{\alpha\beta}^{ref} - \boldsymbol{i}_{\alpha\beta}) \tag{7}$$

According to the power angle based active power control, the grid synchronisation is naturally achieved without using a dedicated synchronisation unit such as PLL. The centred frequency ω used in the current loop is also provided by the output of the power loop controller.

SPC defines the virtual inductance L_{v} and its damping resistance R_v, and hence the current reference in stationary frame is,

$$i_{\alpha\beta}^{ref} = \frac{e_{\alpha\beta} - v_{\alpha\beta}}{R_v + sL_v} \tag{8}$$

where the virtual electromotive force is written as,

$$e_\alpha = E\cos(\omega t) \tag{9}$$

$$e_\beta = E\sin(\omega t) \tag{10}$$

The active power control is designed in detail in the next section for inertia emulation and primary frequency control, while the reactive power controller is written as,

$$E = E_{\text{ref}} + \left(K_{pQ} + \frac{K_{iQ}}{s}\right)(Q_{\text{ref}} - Q) \tag{11}$$

Besides, the reactive power reference Q_{ref} is modified by an outer droop controller written as (12) containing a dead band,

$$Q_{\text{ref}} = Q_{\text{set}} + D_Q[\text{deadband}(V_{\text{ref}} - V)] \tag{12}$$

3 Synchronous active power control loop

Typically the active power loop controller is designed as an emulation of the swing equation of synchronous machines that is written as,

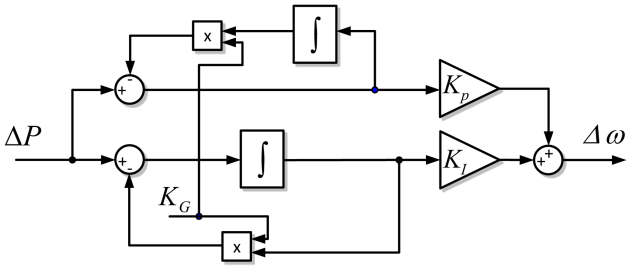

Fig. 2 *Control structure of the power loop controller*

$$P_{\mathrm{m}} - P_{\mathrm{e}} = \left(\frac{2HS_N}{\omega_{\mathrm{s}}}s + D\right)\omega \tag{13}$$

where P_{m} and P_{e} are the mechanical and electrical power, H the inertia constant, S_{N} the nominal power of the generator, ω_{s} the nominal angular speed, D the damping factor and ω the output angular speed.

In case of grid-connected converters, (13) becomes,

$$\omega = \omega_{\mathrm{ref}} + \frac{1}{(2HS_{\mathrm{N}}/\omega_{\mathrm{s}})s + D}(P_{\mathrm{ref}} - P) \tag{14}$$

It is worth noting that the active power loop controller is not necessarily a faithful replication of the swing equation as (14), while different strategies can be used [38]. This paper uses a generalised form integrating the inertia emulation and the *P-f* droop control.

3.1 Design of the loop compensator

The control structure generalising the inertia, damping and *P-f* droop characteristics is shown in Fig. 2.

It is easy to see that the lower part of Fig. 2 realises the swing equation, while an additional upper part is also added in the controller. The objective of this change in the control structure is to add an extra constant to specify the droop slope. The structure shown in Fig. 2 is obtained as a result of the mathematical expression written as,

$$\omega = \omega_{\mathrm{ref}} + \frac{K_{\mathrm{P}}s + K_{\mathrm{I}}}{s + K_{\mathrm{G}}}(P_{\mathrm{ref}} - P) \tag{15}$$

Then the active power loop transfer function is written as,

$$\frac{\partial P}{\partial P_{\mathrm{ref}}}(s) = \frac{(2\xi\omega_n - K_{\mathrm{G}})s + \omega_n^2}{A(s)} \tag{16}$$

where the characteristic equation $A(s)$ can be expressed by a second-order parametric equation as,

$$A(s) = s^2 + 2\xi\omega_n s + \omega_n^2. \tag{17}$$

In (17) the damping factor ξ and natural frequency ω_n are defined by,

$$\xi = \frac{P_{\max}K_{\mathrm{P}} + K_{\mathrm{G}}}{2\sqrt{P_{\max}K_{\mathrm{I}}}} \tag{18}$$

$$\omega_n = \sqrt{P_{\max}K_{\mathrm{I}}}. \tag{19}$$

To relate the natural frequency ω_n in (16) to the inertia constant to explicitly indicate the inertia characteristics, the power loop transfer function based on the swing equation emulation (14) is also derived and written as,

$$\frac{\partial P_{\mathrm{e}}}{\partial P_{\mathrm{m}}}(s) = \frac{(P_{\max}\omega_{\mathrm{s}}/2HS_{\mathrm{N}})}{s^2 + (D\omega_{\mathrm{s}}^2/2HS_{\mathrm{N}})s + \frac{P_{\max}\omega_{\mathrm{s}}}{2HS_{\mathrm{N}}}} \tag{20}$$

Then the controller gain K_{I} can be written in terms of the inertia constant as (21), which is derived by equating the denominator of (16) and (20).

$$K_{\mathrm{I}} = \frac{\omega_{\mathrm{s}}}{2HS_{\mathrm{N}}} \tag{21}$$

Except for the transfer function between the power reference and the generated power, the response of generated power under frequency perturbations should also be modelled. The P-ω_{g} transfer function is written as,

$$\frac{\partial P}{\partial \omega_{\mathrm{g}}}(s) = \frac{-P_{\max}(s + K_{\mathrm{G}})}{A(s)} \tag{22}$$

Based on (22), the *P-f* droop slope can be calculated as,

$$R_{\mathrm{d}} = \frac{S_{\mathrm{N}}}{|(\partial P/\partial\omega_{\mathrm{g}})(0)\,|\,\omega_{\mathrm{s}}} = \frac{S_{\mathrm{N}}K_{\mathrm{I}}}{\omega_{\mathrm{s}}K_{\mathrm{G}}} \tag{23}$$

R_{d} is the per-unit value of the *P-f* droop slope that describes the deviation of frequency in percentage that results in the change of power in the amount of S_{N}. It is found that R_d is determined by the parameters K_{I} and K_{G}. Since (21) has given the criterion to determine K_{I}, the droop slope will be only determined by K_{G} once K_{I} is fixed. Then the criterion to determine K_{G} is written as,

$$K_{\mathrm{G}} = \frac{1}{2HR_{\mathrm{d}}} \tag{24}$$

Substituting K_{I} and K_{G} in (18) using (21) and (24), the expression of K_{P} is obtained as,

$$K_{\mathrm{P}} = 2\xi\sqrt{\frac{\omega_{\mathrm{s}}}{2HS_{\mathrm{N}}P_{\max}}} - \frac{1}{2HR_{\mathrm{d}}P_{\max}} \tag{25}$$

In summary, the parameters K_{P}, K_{I} and K_{G} can set the damping, inertia and droop characteristics, respectively.

3.2 Local stability

As an important design consideration, the influence of the control parameters on the local stability should be analysed. For a synchronous machine, the angle stability is mainly determined by the damping factor ξ. In case of a grid-connected converter controlled by the proposed controller, even if the numerator of the power loop transfer function is slightly changed, the characteristic equation remains the same. It is grounded to expect that the local stability is mainly influenced by the damping factor.

Fig. 3 validates the influence of the damping factor ξ on the power loop stability. It shows the root loci with respect to the change of ξ and H. The figure is plotted based on a 5% droop slope. Complying with the Lyapunov first method, the damping factor ξ has to be specified greater than 0 to yield two poles with negative real parts for an asymptotically stable system. Different from the synchronous machines whose damping is limited by some mechanical and electrical constraints, ξ can be tuned to an optimal value for a grid-connected converter. Fig. 3 also shows that the poles move to the right as the inertia constant increases, while they stay in the left half plane in the common range of the inertia constant.

Thanks to the inertia effect of the power loop (by specifying a proper inertia constant), the reference of the current loop does not experience fast changes, and the dynamics of the current loop and the non-linearity of the plant are much less coupled in the

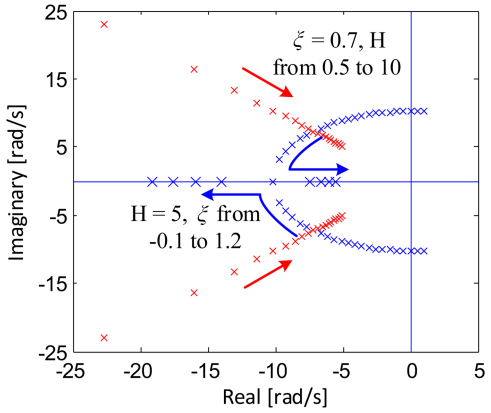

Fig. 3 *Root loci with respect to the damping factor and inertia constant*

3.3 Transient response

The transient response of the active power control loop is evaluated by implementing a unitary step input to the closed-loop system written as,

$$P_{\text{ref}}(t) = 1_A(t) = \begin{cases} 0 & t < 0 \\ \frac{1}{2} & t = 0 \\ 1 & 0 < t <= 3\,\text{s} \end{cases} \tag{27}$$

and the overshoot and settling time of the response are taken as the performance indicators.

The overshoot is calculated following,

$$P_{\text{os}} = \max\left[\frac{P(t)}{P_{\text{ss}}} - 1\right] \tag{28}$$

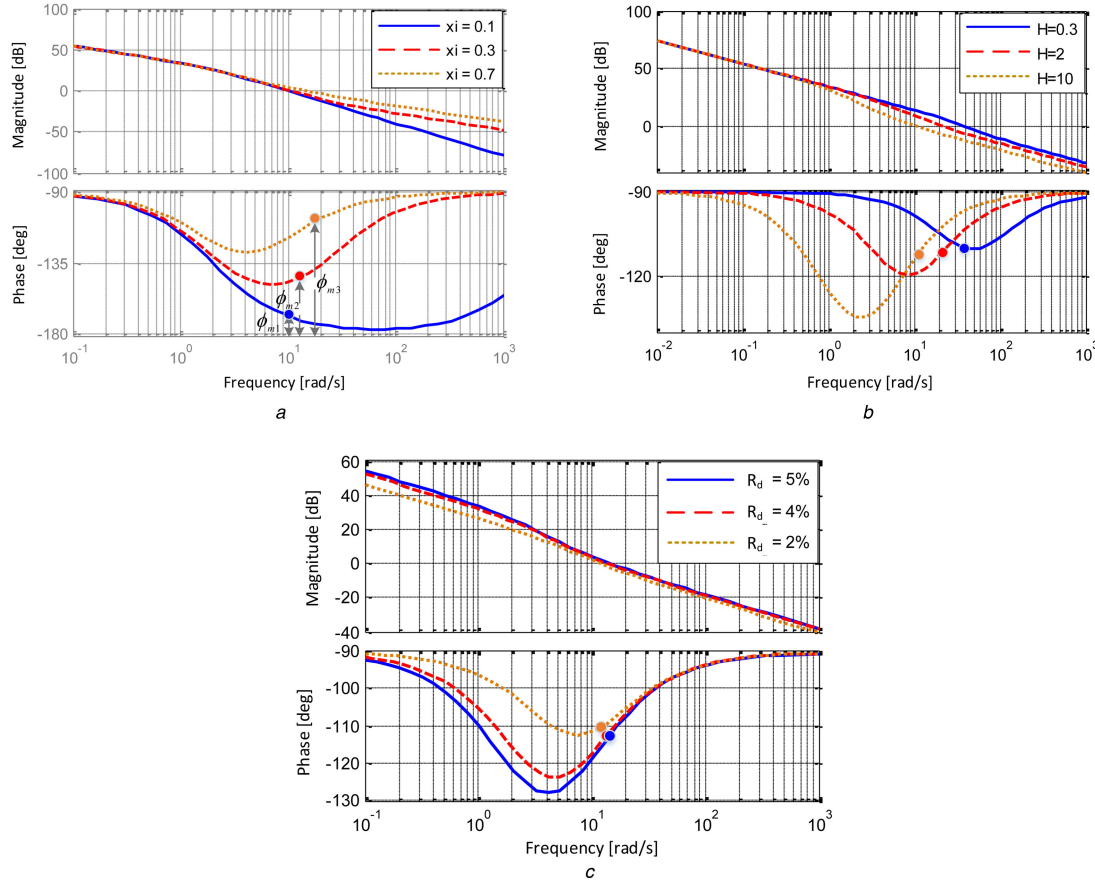

Fig. 4 *Influence of the damping factor, inertia constant and droop slope on the system phase*
(a) Influence of the damping factor, ***(b)*** Influence of the inertia constant, ***(c)*** Influence of the droop slope

dynamics of the active power control. Hence the open-loop system is defined by,

$$G_{\text{OL}}(s) = \frac{K_{\text{P}}s + K_{\text{I}}}{s + K_{\text{G}}} \cdot \frac{1}{s} \cdot \frac{EV}{X} \tag{26}$$

where the virtual admittance and the inner current controller are simply modelled based on (3).

Fig. 4 shows the change of the open-loop system phase affected by the damping factor, inertia constant and droop slope. It is found that the damping factor has a dominant influence on the system phase margin, while the inertia constant and droop slope can be specified considering the requirement of the transmission system operator and the available power reserve without affecting the system stability.

where P_{ss} is the steady-state value obtained at $t = 3$ s. The settling time is calculated following,

$$t_{\text{s}} = T_{\text{s}} \max\left[\forall t \quad \text{s.t.} \quad \left|\frac{P(t)}{P_{\text{ss}}} - 1\right| > \varepsilon_{\text{s}}\right] \tag{29}$$

where T_{s} is the time interval between two adjacent points and ε_{s} is the steady-state band.

H, ξ and R_{d} are specified with multiple values to define the system. According to (20), it is easy to find that the settling time

$$t_{\text{s}} \propto \frac{1}{\omega_n} \propto \sqrt{H} \tag{30}$$

Fig. 5*a* shows that the settling time increases as the inertia constant increases and follows this relation. Fig. 5*b* shows that the damping factor and droop slope have minor influence on t_{s} except that t_{s}

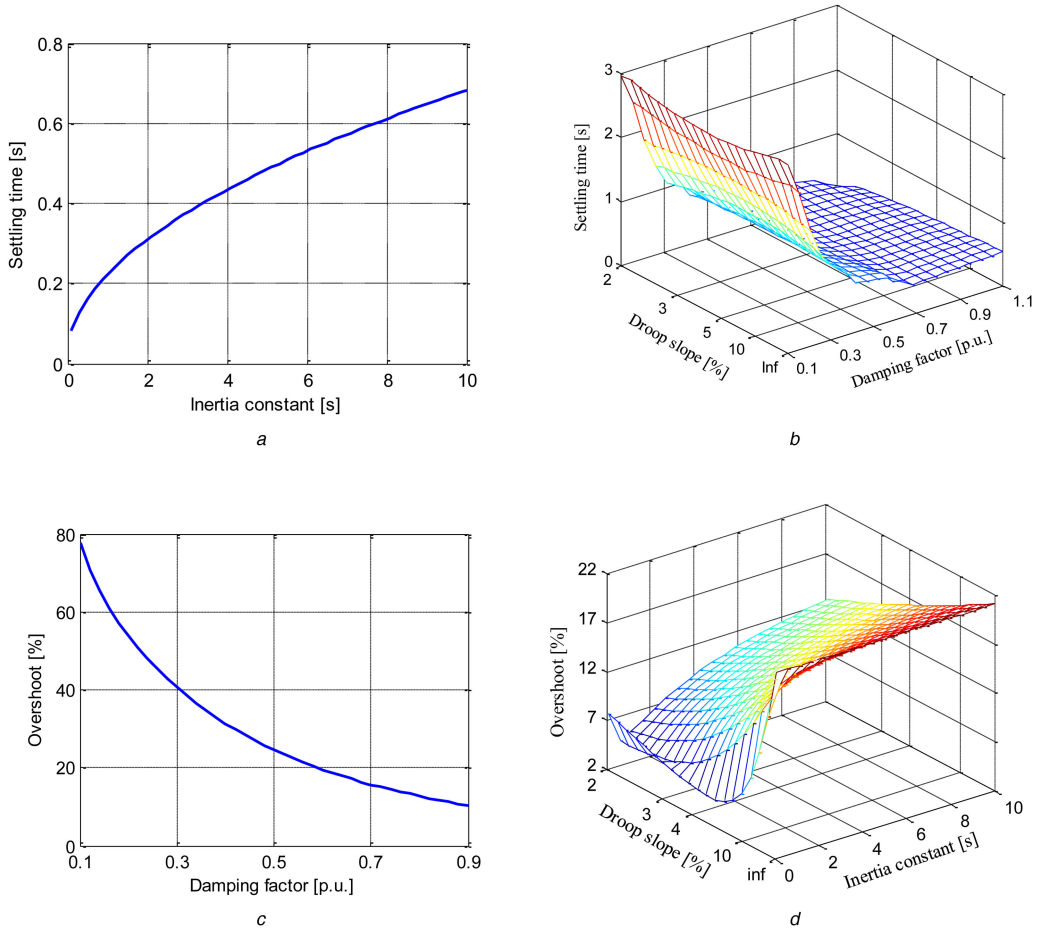

Fig. 5 *Influence of the control parameters on the transient response settling time and overshoot*

(a) Influence of the inertia constant on settling time, ***(b)*** Influence of the damping factor and droop slope on settling time, ***(c)*** Influence of the damping factor on overshoot, ***(d)*** Influence of the inertia constant and droop slope on overshoot

increases significantly when a poor damping is given. Fig. 5*c* shows that the damping factor has a considerable influence on the overshoot of the transient response. It can be concluded that ξ should be not only greater than zero to guarantee the stability, a limit of overshoot should also be set, and further the control parameter K_{P} is tuned. Fig. 5*d* shows that the overshoot also increases along with the inertia constant. However, this trend is limited in an acceptable range under a fixed value of ξ. The droop slope has only minor influence on the overshoot. It is shown that the integration of the droop control in the power loop controller does not introduce any effect on the dynamics. The transient response is still characterised by ξ and H, while R_{d} mainly determine the steady-state performance.

Table 1 Key parameters of the test plant and controller

Parameter	Description	Value
V_{dc}, V	dc bus voltage	640
L_o, mH	converter side inductance	2.6
L_{g}, μH	grid side inductance	662
C_o, μF	filter capacitance	5.5
C_{t}, μF	trap filter capacitance	1
L_{t}, μH,	trap filter inductance	244
R_{co}, Ω	filter damping resistance	1
S_{N}, kW	rated power	10
f_{sw}, Hz	switching frequency	10,050
f_{s}, Hz	sampling frequency	10,050
U_{g}, V	grid line-to-line voltage	400
f_{g}, Hz	grid frequency	50
X_{pu}, p.u.	per-unit virtual reactance	0.3
R_{pu}, p.u.	per-unit virtual resistance	0.1
ξ	damping factor	0.7

4 Simulation results

Simulation tests are conducted to show the performance of the proposed control strategy in grid frequency support. A 10 kW two-level three-phase grid-connected converter is built in the simulation model. The converter is connected to the grid through a LCL-trap filter [39]. In order to show the response of the active power as a function of the grid frequency changes, a Thevenin model is used to form the grid. The three-phase voltage is generated by *dq* transformation of the voltage magnitude, and the phase angle is an integration of the programmed frequency. The controller is discretised and coded in a simplified c block to minimise the gap between the simulation and the experimental implementation. The parameters of the plant and the controller are shown in Table 1 (same to the parameters of the experimental setups).

A ramp change of the grid frequency is implemented in the test as shown in Fig. 6*a*, and the response of the active power is measured. The test is repeated for several times with different values in inertia constant and droop slope, and the damping factor is kept unchanged. Fig. 6*b* compares the profiles from different cases.

During the change of the grid frequency, the active power injection accordingly changes to resist the frequency deviation and give frequency support. In three different cases the droop slope R_{d} is specified to 5 and 10% and infinite ($K_{\mathrm{G}} = 0$) while the inertia constant H is fixed to 10 s. It is shown that the steady-state value of active power reaches 0.64, 0.62 and 0.6, respectively. Considering that the deviation of grid frequency is 0.1 Hz, the steady-state active power injection matches with the specified droop slope. For

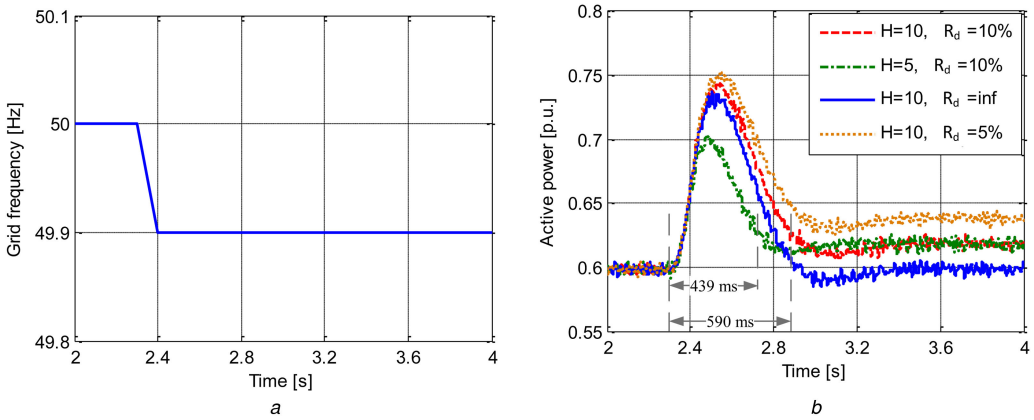

Fig. 6 *Simulated transient response under different inertia constant and droop slope*
(a) Grid frequency changes, ***(b)*** Active power response

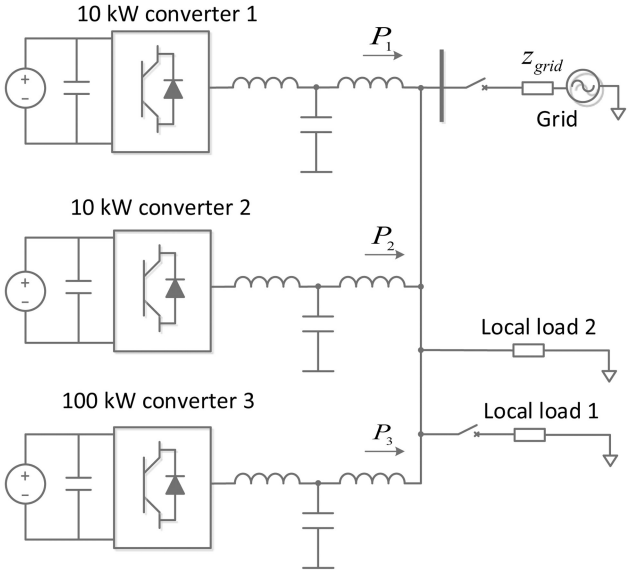

Fig. 7 *Simulated system for validating the load sharing of parallel connected converters*

evaluating the inertia characteristics, R_d is fixed to 10%, and H is assigned to 5 and 10 s in two cases. Because of the same value in R_d, two profiles reaches the same steady-state value (0.62). The settling time of the two responses are calculated considering a steady-state band of 5%. The settling time when $H = 10$ s is 590 ms, and the settling time when $H = 5$ s is 439 ms. It validates the relation (30). In summary, the specified inertial dynamics and droop slope can both be achieved using the proposed synchronous active power control loop.

The power sharing capability of the SPC is validated as follow. Fig. 7 shows the simulated setup with three parallel connected converters. Two of them are 10 kW converters and the third one is 100 kW. A switch determines the operation mode (island or grid connection), and the resistive local loads of 120 kW are also connected at the point of connection. The virtual admittance of each converter has the same per-unit value (0.3), and then the loads can be shared according to the weight (power rating) of each converter.

The initial operation point of the three converters are 8, 6 and 70 kW, and the remaining part of the loads are supplied by the grid. At $t = 1.2$ s, the grid connection switch is opened, and at $t = 1.6$ s 40 kW of loads are shedded. The grid voltage, load voltage and current injection of each converter are shown in Fig. 8, and the power calculation of each converter and the loads are shown in Fig. 9.

During the islanding and load shedding, the load voltage does not experience significant change, demonstrating the grid forming ability. At $t = 1.2$ s, three converters accordingly increase the power to balance the local loads. The power increase of the three converters are around 2, 2 and 20 kW, respectively, which are proportional to their power ratings. After the islanding, the load power is slightly reduced because of the minor decrease in the load voltage magnitude. At $t = 1.6$, the power generation of each converter reduces because of the load shedding. The power changes are proportional to their power ratings, and the load voltage is maintained.

The above results show that islanding can be realised smoothly without control scheme switching, and the converters can properly share the loads under load changes.

5 Experimental results

The frequency support characteristics are further validated in laboratory test bed. The experimental setups are shown in Fig. 10, where a 10 kW converter interacts with the grid that is formed by the regenerative power source California Instrument MX45. By using this ac source the grid voltage waveforms, magnitude and frequency are programmed, and hence the sweep of grid frequency can be generated. A 20 kW dc power source supplies the dc bus of the converter, the control is implemented in dSPACE ds1103 using the same code used in the simulation tests. The parameters are the same to the simulation parameters as shown in Table 1.

Fig. 11 shows the transient response of active power in presence of grid frequency sweep. Fig. 11*a* shows the programmed frequency sweep, and the ramp slope is ±1 Hz/s. Fig. 11*b* shows the waveforms of the grid voltage and current injected by the converter during the frequency changes. The current is well controlled in steady state and exhibit a significant transient response to oppose the change of the grid frequency. During the transient the response of the converter presents a smooth variation free from oscillations. Fig. 11*c* compares the response of active power obtained by analytical, simulation and experimental study. In the three cases the controller is assigned with the same parameters. In analytical study, the same sweep change is given to the transfer function (22) and the response of P is recorded. Fig. 11*c* shows a perfect match among the responses from the three different cases. It indicates that the transient response of the grid-connected converter in practice is able to follow the dynamics that is analytically specified. In this way, the damping, inertia and droop characteristics can be accurately given and the control is demonstrated to be experimentally feasible. The *P-f* droop slope is fixed to 10% in the test, and the measured active power increases from 0.5 p.u. and stabilises at 0.56 p.u. when the grid frequency holds at 49.7 Hz, and stabilises at 0.44 p.u. when the grid frequency holds at 50.3 Hz. Fig. 11*c* also shows the evolution of the virtual synchronous angular speed ω, it is seen that the high amount of inertia ($H = 10$ s) results in a greater settling time of the grid frequency tracking compared with the conventional PLL. The difference between ω and ω_g during the transient leads to a great change of active power to oppose the frequency deviation and thus presents inertial dynamics.

Fig. 12 compares the transient responses of the converter when different values of H is specified. The frequency change that

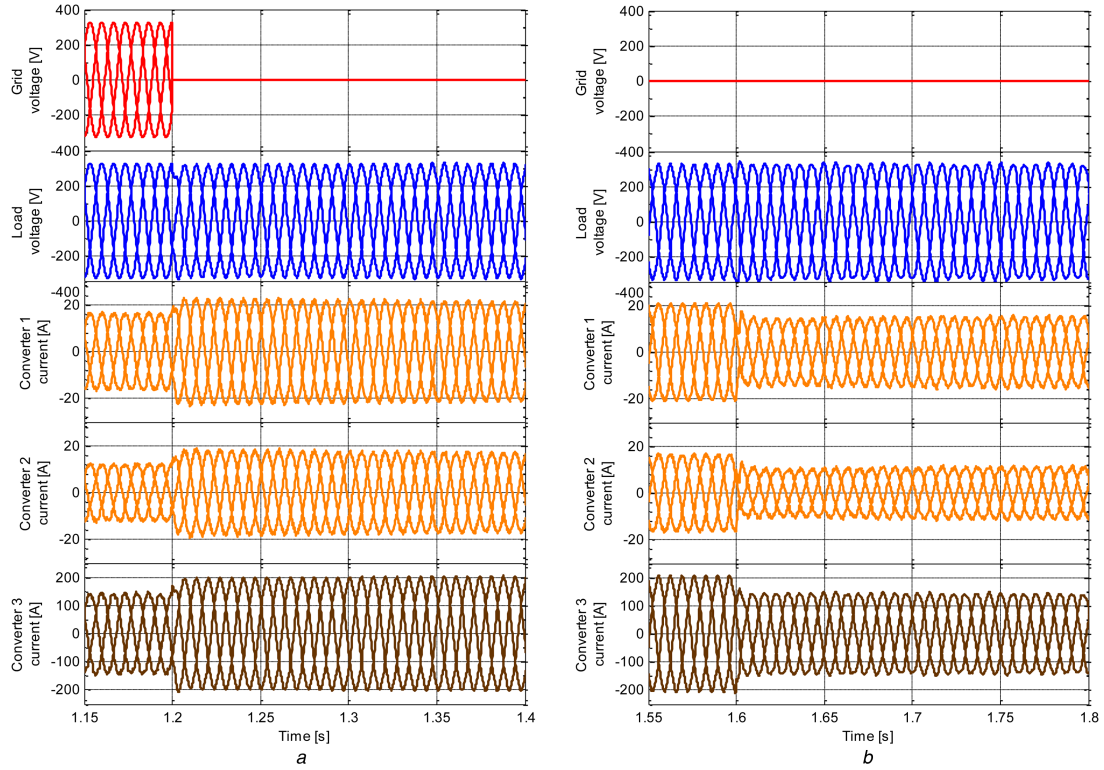

Fig. 8 *Grid voltage, load voltage and current injection of each converter*
(a) Transient during islanding, ***(b)*** Response to load changes

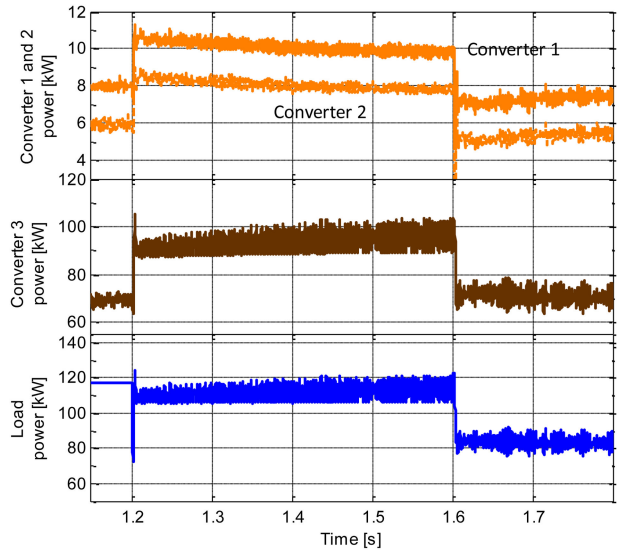

Fig. 9 *Active power generation of each converter and the load power*

triggers the responses is shown in Fig. 12*c*. The ramp slope of the frequency change is ±3 Hz/s. The initial operating point of the converter is 6 kW and 0 kVar. When H is 5 s, the grid voltage and injected current waveforms are shown in Fig. 12*a*, while the ones when H is 10 s are shown in Fig. 12*b*. In both cases the current is well regulated and smoothly changes following inertial dynamics. The active power in both cases are measured and compared with each other in Fig. 12*d*. Two profiles shown in Fig. 12*d* settle at the steady state respectively 944 and 658 ms after the second ramp change of the grid frequency. It is easy to calculate that $944/658 = 1.43 \simeq \sqrt{10/5}$, which matches with (30).

Then the droop characteristics are demonstrated in Fig. 13. The change of the grid frequency is plotted in Fig. 13*b*, where it decreases to 49.9 Hz during 0.1 s, holds for 1 s and increases back to 50 Hz during 0.1 s. In three different cases the droop slope R_{d} is infinite ($K_{\mathrm{G}} = 0$), 10 and 5%, corresponding to 0, 2 and 4 kW/Hz. Fig. 13*a* shows the grid voltage and injected current in three cases, and Fig. 13*c* shows the comparison of the transient active power responses. The steady-state value after the first ramp change is 0.6, 0.62 and 0.64 p.u., which match the specified droop slope.

Fig. 14 shows the performance of the SPC in comparison with the classic control strategy that is based on vector current control, PLL and instantaneous power theory. The PLL is a fast one with the settling time 100 ms. The grid frequency sweep profile is specified as Fig. 14*c*. In order to see the difference on the dynamics under the same steady-state performance, the $P - f$ droop slope of the two strategies are fixed to the same value, namely 2%. According to Figs. 14*a* and *b*, both strategies show an effective control, and are different from each other in the transients. The SPC-based method opposes the grid frequency deviation in the transients more than the classic method, as a result of the inertia characteristics ($H = 10$ s). The evolution of active power is shown in Fig. 14*d*. The steady-state active power change is the same (−3 kW) based on the two strategies. Fig. 14*d* also shows that grid synchronisation of SPC is more stable relative to the classic frequency measurement based on a stationary-frame PLL. Besides, the active and reactive power control has a minor coupling effect, which can be explained by (1) and (2).

As another comparison, the performance of the swing equation emulation controller based on (14) is also tested in experiments. Inertia constant and damping coefficient have been specified to 10 and 0.7 s, respectively. The inherent $P - f$ droop characteristics in the power control loop leads to a droop effect shown in Fig. 15 (0.1 Hz deviation leads to 3 kW change in active power). The frequency sweep profile is specified in a smaller range compared to Fig. 14 to avoid saturating the converter. The inertia characteristics are also shown. It can be concluded that the power loop controller used in this paper (15) leads to similar dynamics to the typically used swing equation emulation (14), and has different droop characteristics. The swing equation emulation needs to modify the droop slope through an additional droop loop.

In summary, the experimental results further verifies the inertia and droop characteristics of the controller in presence of grid frequency changes. The identical transient active power response from the analytical, simulation and experimental results shows the effectiveness and the easy experimental implementation of the designed controller. A controllable transient response is hence demonstrated.

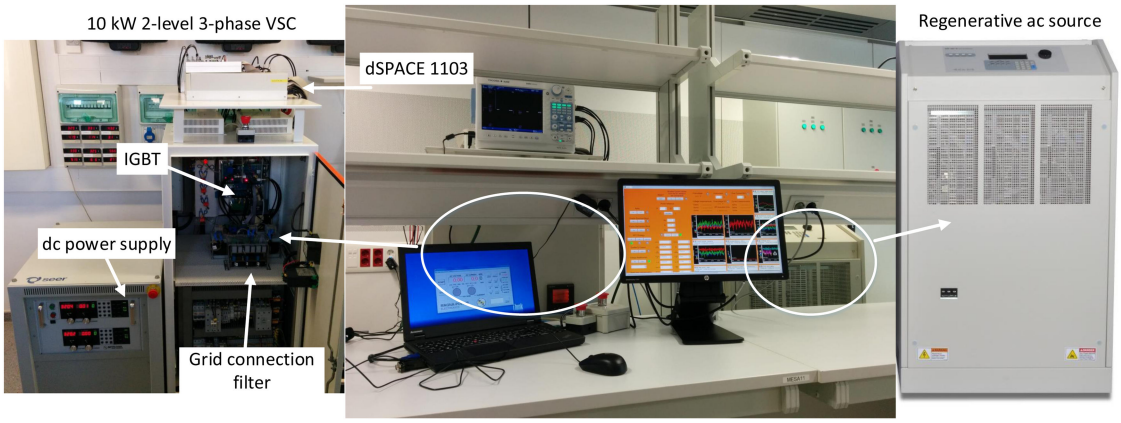

Fig. 10 *10 kW laboratory experimental test bed*

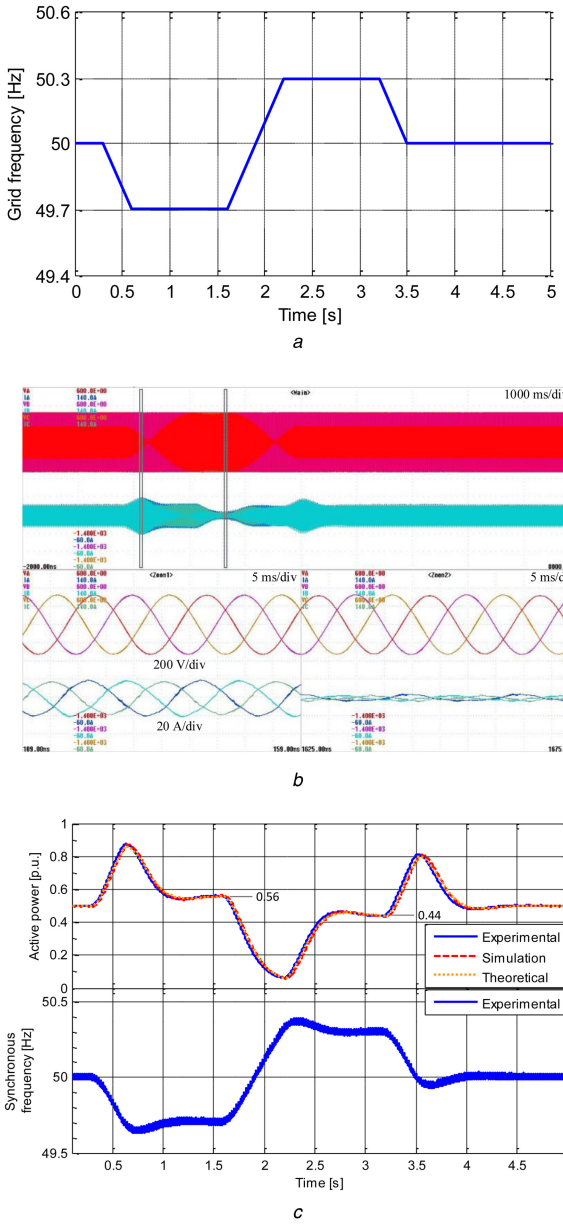

Fig. 11 *Comparison of theoretical, simulated and experimental power response in presence of grid frequency sweep*

(a) Grid frequency changes, ***(b)*** Grid voltage and injected current, ***(c)*** Comparison of theoretical, simulated and experimental power response; virtual synchronous frequency in experiments

6 Conclusion

This paper designed a synchronous active power control strategy for grid-connected converters oriented to inertia emulation and primary frequency control. The power loop controller was designed to incorporate damping, inertia emulation and *P-f* droop characteristics with considerations of stability and dynamics. Frequency support characteristics of the controlled converter were particularly analysed and validated in this paper. The analytical relation between the grid frequency deviation and the active power change was derived based on the accurate modelling of the active power control loop. The simulation and experimental tests were done on a 10 kW regenerative source test bed. The inertia and droop characteristics were clearly shown in frequency sweep tests when the converter is controlled by different sets of parameters. The test results present the identical responses as theoretically specified. Therefore, the inertia constant, damping factor and droop slope can be accurately given for good grid-interaction dynamics. The consistency shows the easy implementation of the proposed controller, as a step toward the future field tests.

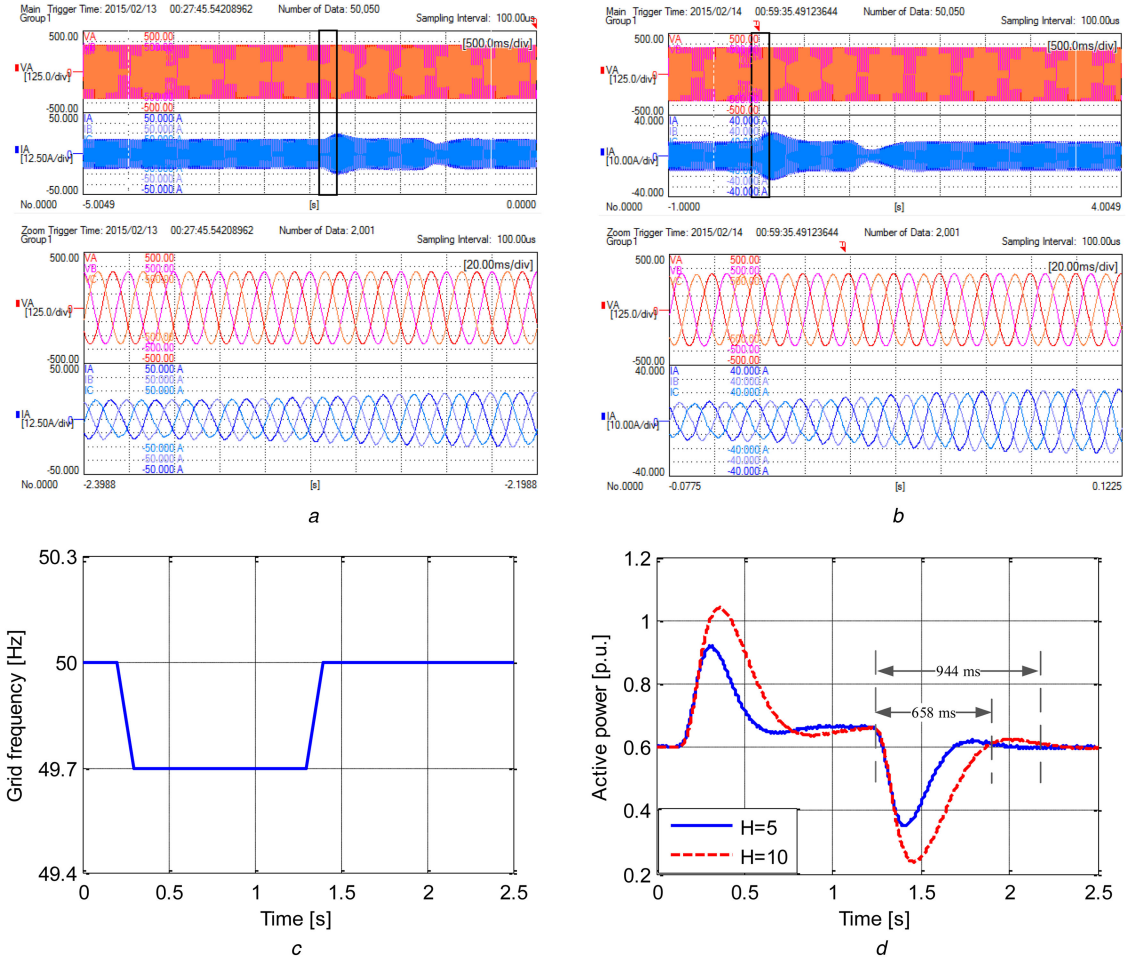

Fig. 12 *Comparison of the transient response under different inertia constant*

(a) Grid voltage and injected current when $H = 5$, ***(b)*** Grid voltage and injected current when $H = 10$, ***(c)*** Grid frequency changes, ***(d)*** Comparison of active power response

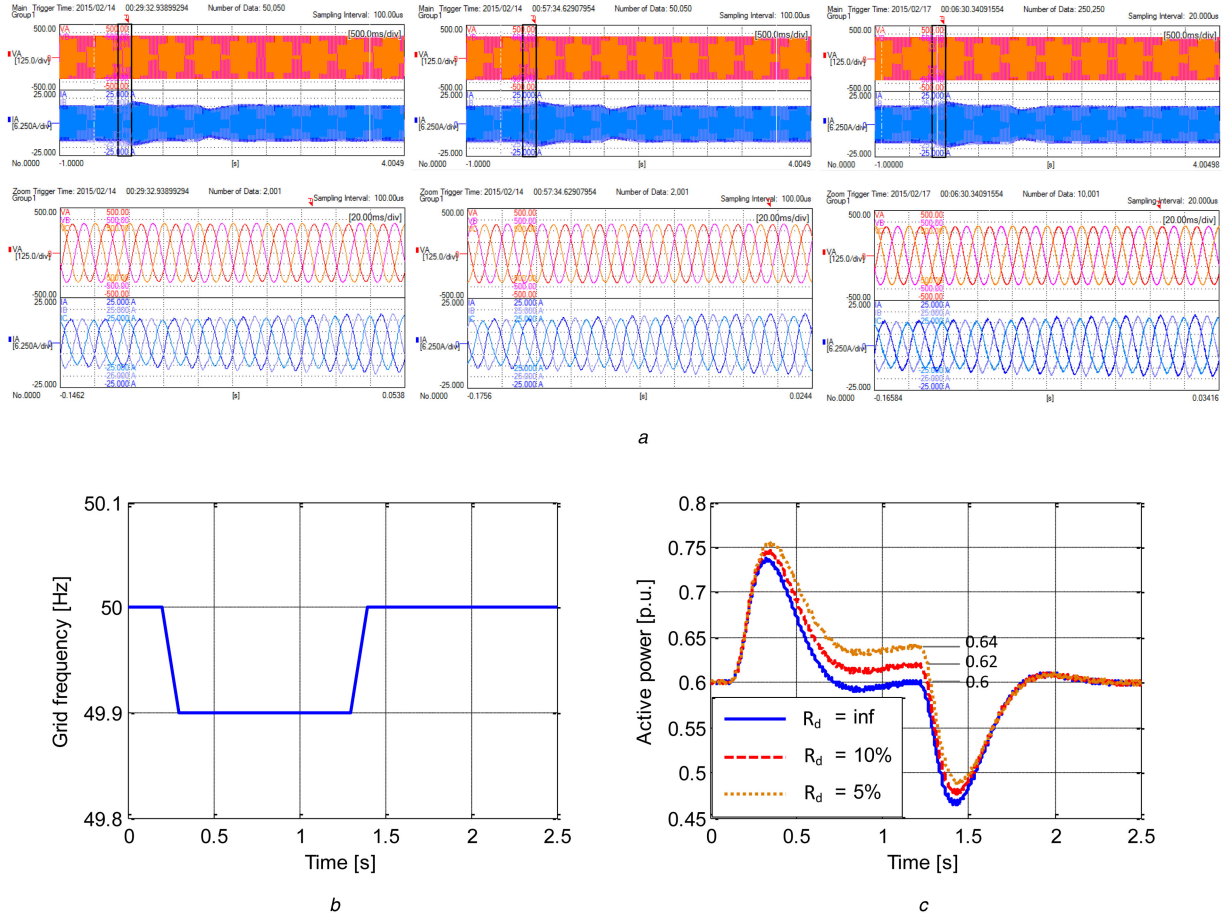

Fig. 13 *Comparison of the transient response under different droop slope*

(a) Grid voltage and injected current under different droop slope, ***(b)*** Grid frequency changes, ***(c)*** Comparison of active power response

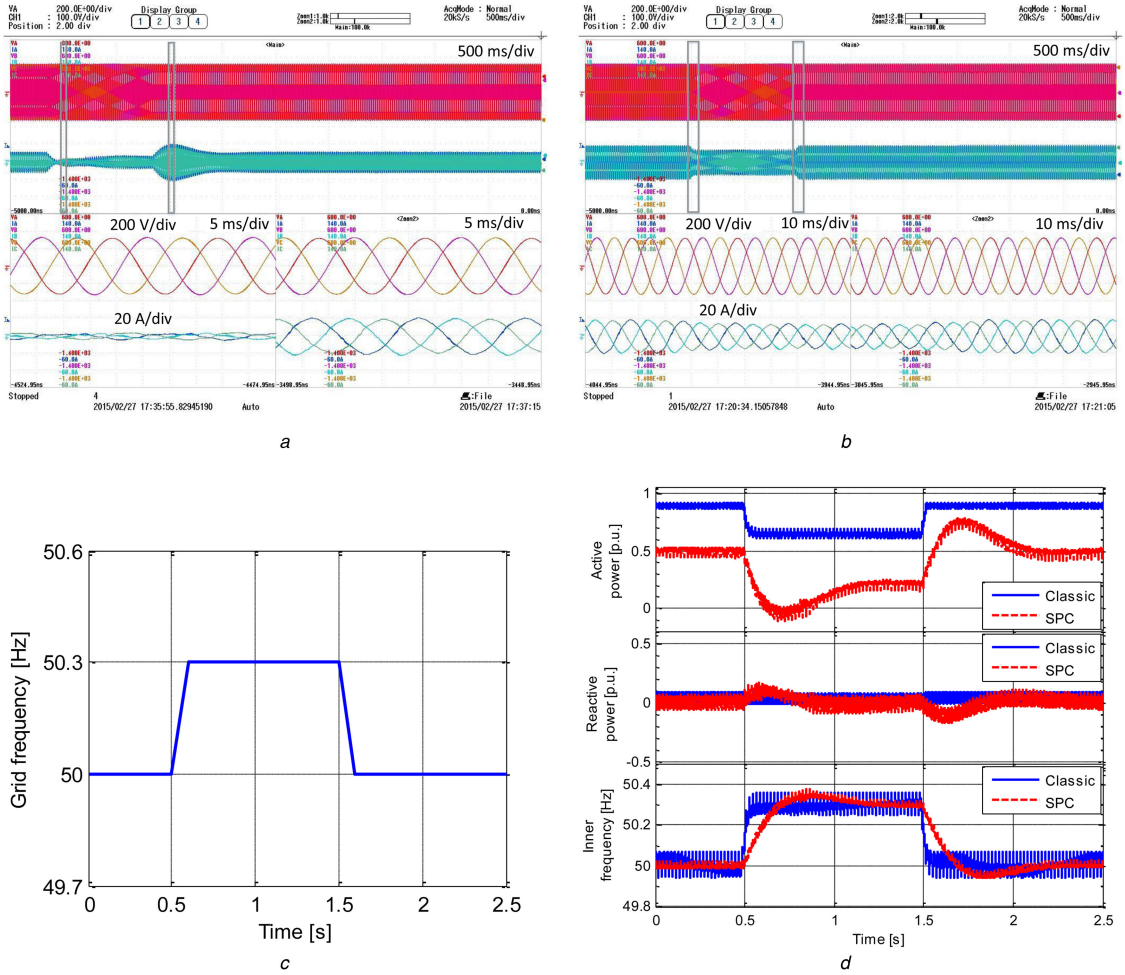

Fig. 14 *Comparison between the SPC and classic instantaneous power vector current control under frequency sweep*
(a) Voltage and current under SPC control, ***(b)*** Voltage and current under classic control, ***(c)*** Grid frequency, ***(d)*** Comparison of active power, reactive power and inner frequency

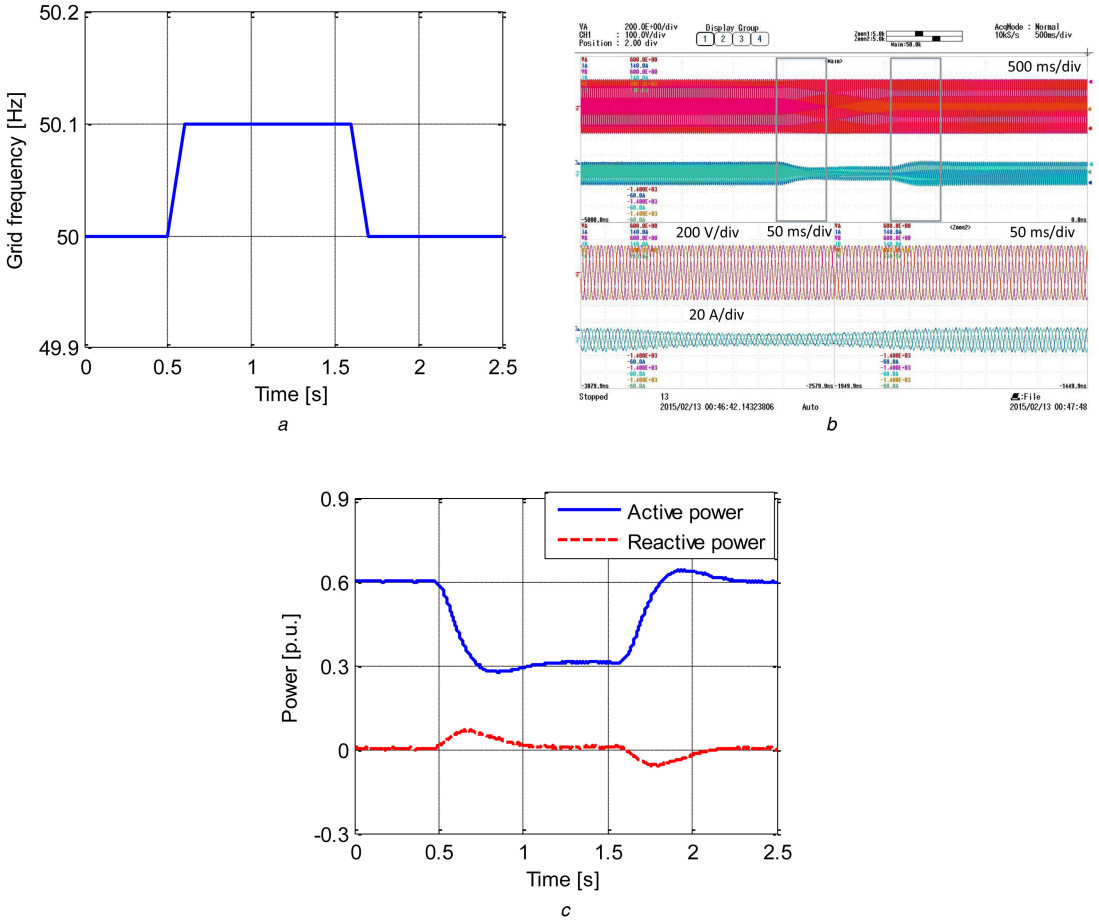

Fig. 15 *Swing equation emulation control under grid frequency sweep*
(a) Grid frequency, ***(b)*** Voltage and current, ***(c)*** Active and reactive power

7 References

[1] ENTSOE: 'ENTSO-E network code for requirements for grid connection applicable to all generators'. 2013

[2] Driesen, J., Visscher, K.: 'Virtual synchronous generators'. IEEE PES General Meeting, 2008, pp. 1–3

[3] Han, H., Hou, X., Yang, J., *et al.*: 'Review of power sharing control strategies for islanding operation of AC microgrids', *IEEE Trans. Smart Grid*, 2016, **7**, (1), pp. 200–215

[4] Bhattacharya, S., Mishra, S.: 'Efficient power sharing approach for photovoltaic generation based microgrids', *IET Renew. Power Gener.*, 2016, **10**, (7), pp. 973–987

[5] Ramezani, M., Li, S., Sun, Y.: 'Combining droop and direct current vector control for control of parallel inverters in microgrid', *IET Renew. Power Gener.*, 2016

[6] Teodorescu, R., Liserre, M., Rodriguez, P.: '*Grid converters for photovoltaic and wind power systems*' (John Wiley & Sons, Ltd, 2011)

[7] Akagi, H., Hirokazu, E., Aredes, M.: '*Instantaneous power theory and applications to power conditioning*' (John Wiley & Sons, Ltd, 2007)

[8] Liu, J., Miura, Y., Ise, T.: 'Comparison of dynamic characteristics between virtual synchronous generator and droop control in inverter-based distributed generators', *IEEE Trans. Power Electron.*, 2016, **31**, (5), pp. 3600–3611

[9] Arco, S.D., Suul, J.A.: 'Equivalence of virtual synchronous machines and frequency-droops for converter-based microGrids', *IEEE Trans. Smart Grid*, 2014, **5**, (1), pp. 394–395

[10] Hesse, R., Beck, H.P., Turschner, D.: 'Conditioning device for energy supply networks'. United States Patent US008510090B2, October 2007

[11] Beck, H.P., Hesse, R.: 'Virtual synchronous machine'. Proc. EPQU, 2007, pp. 1–6

[12] Van Wesenbeeck, M.P.N., De Haan, S.W.H., Varela, P., *et al.*: 'Grid tied converter with virtual kinetic storage'. IEEE Bucharest PowerTech, 2009, pp. 1–7

[13] Zhong, Q.C., Weiss, G.: 'Synchronverters: Inverters that mimic synchronous generators', *IEEE Trans. Ind. Electron.*, 2011, **58**, (4), pp. 1259–1267

[14] Zhang, L., Harnefors, L., Nee, H.P.: 'Power-synchronization control of grid-connected voltage-source converters', *IEEE Trans. Power Syst.*, 2010, **25**, (2), pp. 809–820

[15] Zhong, Q.C., Nguyen, P., Ma, Z., *et al.*: 'Self-synchronized synchronverters : inverters without a dedicated synchronization unit', *IEEE Trans. Power Electron.*, 2014, **29**, (2), pp. 617–630

[16] Sakimoto, K., Miura, Y., Ise, T.: 'Stabilization of a power system with a distributed generator by a virtual synchronous generator function'. ICPE 2011-ECCE Asia, 2011, pp. 1498–1505

[17] Chen, Y., Hesse, R., Turschner, D., *et al.*: 'Comparison of methods for implementing virtual synchronous machine on inverters'. Proc. ICREPQ, 2012, pp. 1–6

[18] Rodriguez, P., Candela, I., Citro, C., *et al.*: 'Control of grid-connected power converters based on a virtual admittance control loop'. Proc. EPE, 2013, pp. 1–6

[19] Torres, M.A., Lopes, L.A., Moran, L.A., *et al.*: 'Self-tuning virtual synchronous machine : A control strategy for energy storage systems to support dynamic frequency control', *IEEE Trans. Energy Convers.*, 2014, **29**, (4), pp. 833–840

[20] Alipoor, J., Miura, Y., Ise, T.: 'Power system stabilization using virtual synchronous generator with alternating moment of inertia', *IEEE J. Emerg. Sel. Top. Power Electron.*, 2015, **03**, (2), pp. 451–458

[21] Vrana, T.K., Hille, C.: 'A novel control method for dispersed converters providing dynamic frequency response', *Electr. Eng.*, 2011, **93**, (4), pp. 217–226

[22] D'Arco, S., Suul, J.A., Fosso, O.B.: 'Control system tuning and stability analysis of Virtual Synchronous Machines'. IEEE Energy Conversion Congress Exposition (ECCE), 2013, pp. 2664–2671

[23] Albu, M., Visscher, K., Creanga, D., *et al.*: 'Storage selection for DG applications containing virtual synchronous generators'. IEEE Bucharest PowerTech, 2009, pp. 1–6

[24] Gao, F., Iravani, M.R.: 'A control strategy for a distributed generation unit in grid-connected and autonomous modes of operation', *IEEE Trans. Power Deliv.*, 2008, **23**, (2), pp. 850–859

[25] Alatrash, H., Mensah, A., Mark, E., *et al.*: 'Generator emulation controls for photovoltaic inverters', *IEEE Trans. Smart Grid*, 2012, **3**, (2), pp. 996–1011

[26] Ashabani, S.M., Mohamed, Y.A.R.I.: 'A flexible control strategy for grid-connected and islanded microgrids with enhanced stability using nonlinear microgrid stabilizer', *IEEE Trans. Smart Grid*, 2012, **3**, (3), pp. 1291–1301

[27] Hirase, Y., Abe, K., Sugimoto, K., *et al.*: 'A grid-connected inverter with virtual synchronous generator model of algebraic type', *Electr. Eng. Japan (English Transl. Denki Gakkai Ronbunshi)*, 2013, **184**, (4), pp. 10–21

[28] Nanou, S.I., Papakonstantinou, A.G., Papathanassiou, S.A.: 'A generic model of two-stage grid-connected PV systems with primary frequency response and inertia emulation', *Electr. Power Syst. Res.*, 2015, **127**, pp. 186–196

[29] Ashabani, M., Freijedo, F.D., Golestan, S., *et al.*: 'Inducverters: PLL-less converters with auto-synchronization and emulated inertia capability', *IEEE Trans. Smart Grid*, 2016, **7**, (3), pp. 1660–1674

[30] Wang, S., Hu, J., Yuan, X.: 'Virtual synchronous control for grid-connected DFIG-based wind turbines', *IEEE J. Emerg. Sel. Top. Power Electron.*, 2015, **3**, (4), pp. 932–944

[31] Zhang, L., Harnefors, L., Nee, H.P.: 'Interconnection of two very weak AC systems by VSC-HVDC links using power-synchronization control', *IEEE Trans. Power Syst.*, 2011, **26**, (1), pp. 344–355
[32] Zhu, J., Booth, C.D., Adam, G.P.*, et al.*: 'Inertia emulation control strategy for VSC-HVDC transmission systems', *IEEE Trans. Power Syst.*, 2013, **28**, (2), pp. 1277–1287
[33] Guan, M., Pan, W., Zhang, J.*, et al.*: 'Synchronous generator emulation control strategy for voltage source converter (VSC) stations', *IEEE Trans. Power Syst.*, 2015, **30**, (6), pp. 3093–3101
[34] Zhang, W., Rouzbehi, K., Luna, A.*, et al.*: 'Multi-terminal HVDC grids with inertia mimicry capability', *IET Renew. Power Gener.*, 2016, pp. 1–9
Q2 [35] Chen, Y., Hesse, R., Turschner, D.*, et al.*: 'Dynamic properties of the virtual synchronous machine (VISMA)'. Proc. ICREPQ, 2011, pp. 1–5
[36] Rodriguez, P., Candela, I., Rocabert, J.*, et al.*: 'Synchronous power controller for a generating system based on static power converters'. International Patent WO 2012/117 131 A1, 7 September 2012, Priority date: 18 February 2011, Licensed by: Abengoa S.A.
[37] Rodriguez, P., Candela, I., Luna, A.: 'Control of PV generation systems using the synchronous power controller'. IEEE Energy Conversion Congress Exposition (ECCE), 2013, pp. 993–998
[38] Zhang, W., Remon, D., Mir, A.*, et al.*: 'Comparison of different power loop controllers for synchronous power controlled grid-interactive converters'. IEEE Energy Conversion Congress Exposition (ECCE), 2015, pp. 3780–3787
[39] Cantarellas, A.M., Rakhshani, E., Remon, D.*, et al.*: 'Design of the LCL + trap filter for the two-level VSC installed in a large-scale wave power plant'. IEEE Energy Conversion Congress Exposition (ECCE), 2013, pp. 707–712